The fracture toughness and fatigue crack propagation behaviour of annealed PET

T. J. Pecorini* and R. W. Hertzberg
Department of Materials Science and Engineering, Lehigh University, Bethlehem, PA 18015, USA
(Received 13 July 1992; revised 15 December 1992)

The fracture toughness of poly(ethylene terephthalate) (PET) is correlated with various morphologies produced upon annealing. Annealing PET at a Hoffman regime III crystallization temperature (120°C) or inducing solid-state polymerization result in materials of high fracture toughness ($K_c = 8.7$ MPa $m^{1/2}$ and 9.5 MPa $m^{1/2}$, respectively); these high toughness values are related to multiple-crazing mechanisms produced by high tie-molecule densities. Annealing fully dried PET at 200°C transforms the material to a Hoffman regime I/II structure, and the fracture toughness decreases to 6.5 MPa $m^{1/2}$. Hydrolysis also reduces the fracture toughness ($K_c < 3$ MPa $m^{1/2}$). In these low toughness materials, multiple crazing is not observed. In addition, the fatigue crack propagation response of PET is found to be superior in samples annealed to produce high fracture toughness as compared with samples annealed to produce low fracture toughness values.

(Keywords: annealing; poly(ethylene terephthalate); fracture toughness)

INTRODUCTION

The strength, ductility and toughness of engineering polymers vary greatly according to thermal treatment. Unfortunately, in the case of step-polymerized semicrystalline resins, such as poly(ethylene terephthalate) (PET), these thermal treatments may induce distinct and simultaneous changes in both molecular weight and the amount and perfection of the crystalline phase. In order to characterize the relationship between thermal treatment and mechanical properties, these separate transformations must be isolated and subsequently related to the manner in which they affect load transfer through the material.

The mechanical properties of semicrystalline polymers are controlled by the number of links between the crystalline lamellae[1-8]. When tie-molecule density is high, lamellar shear occurs before the tie molecules fracture, and a craze develops (see *Figure 1a*). An ample supply of tie molecules will intensity multiple crazing and extend the craze network, thereby enhancing polymer ductility. Fracture toughness and fatigue resistance, which are related to both strength and ductility, are improved when the craze network is stabilized by a large tie-molecule density.

If, however, the tie-molecule density is low, the concentrated load transmitted through these links will produce molecular fracture. In this situation, the stress on the adjacent lamellae is not large enough to produce significant lamellar shear, whereby macroscopically brittle (i.e. low toughness) fracture occurs (*Figure 1b*). (Extended chain crystals, which contain no tie molecules, are well known to be brittle[1,9].)

The tie-molecule density can be regulated by altering the molecular weight of the resin. High-molecular-weight chains will exhibit a greater degree of meandering between lamellae than will short chains and, therefore, the number of interlamellar linkages will be greater[1-3]. In a step-polymerized resin such as PET, the molecular weight can be reduced during an anneal through hydrolysis, or increased through solid-state polymerization[9-14]. Hydrolysis is especially detrimental to the mechanical properties of semicrystalline systems since it occurs preferentially within the amorphous interlamellar regions where the water levels are highest. As a result of hydrolysis, the interlamellar tie-molecule density is reduced and the properties degrade[12,13].

The tie-molecule density can also be affected by crystallization conditions, as predicted with a time–temperature transformation curve (e.g. see *Figure 2*). In the high-temperature portion of this 'C-curve', which Hoffman defines as regimes I and II, reptation rates are high but the crystallization rate is limited by low nucleation rates[9,15-17] (see crystallization paths A and D). Within regimes I/II, the polymer chains crystallize by regular folding, a process by which an entire chain can be deposited within one lamella (*Figure 3a*)[16-18]. Regularly folded structures possess few tie molecules and are expected to exhibit low toughness.

In the low-temperature portion of the C-curve (Hoffman regime III[18,19]), nucleation rates are high but diffusion is sluggish (see crystallization paths B and E). The polymer chains crystallize by freezing in place and retain their amorphous radii of gyration. Hoffman notes that, within regime III, the polymer chains exhibit much meandering and a low degree of folding (see *Figure 3b*)[18]. This variable cluster conformation contains many tie molecules and should produce a tough polymer.

The objective of this investigation is to review changes

* To whom correspondence should be addressed. Present address: Eastman Chemical Co., PO Box 1972, Kingsport, TN 37662, USA

0032-3861/93/245053-10

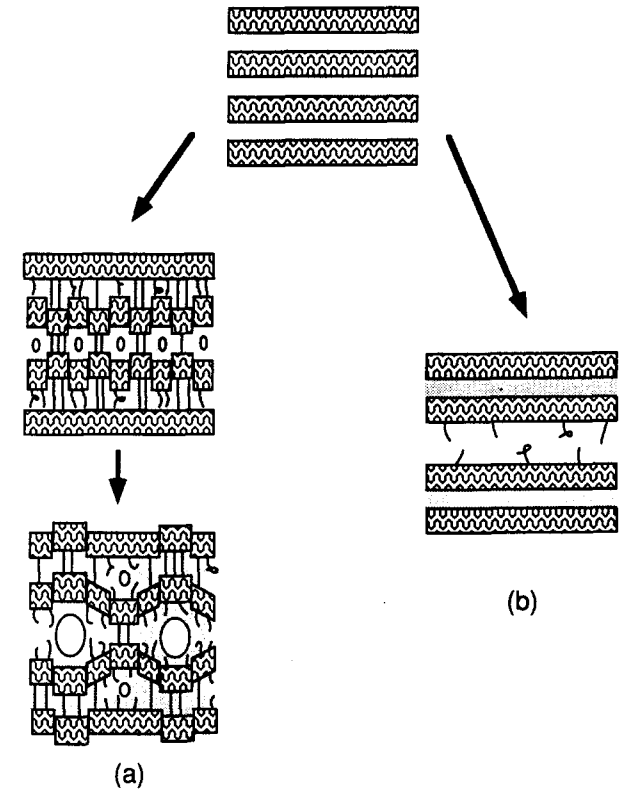

Figure 1 Modes of fracture in a semicrystalline polymer. (a) High-tie molecule density leads to lamellar shear and crazing, i.e. ductile fracture. (b) Low tie-molecule density leads to brittle fracture

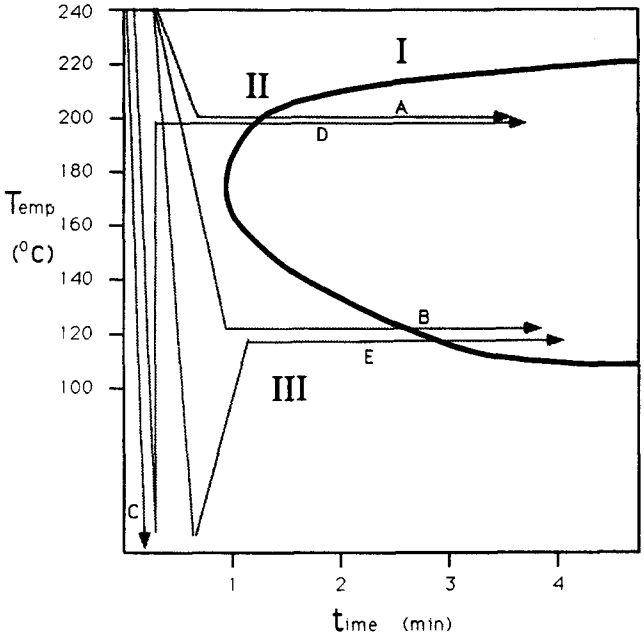

Figure 2 Typical crystalline 'C-curve' for polymers showing time to crystallize at various temperatures. Paths A and B represent isothermal crystallization. Path C represents a rapid quench. Paths D and E represent annealing processes following a rapid quench. Path A will produce large spherulites; paths B, D and E will produce a fine spherulitic structure; path C leads to amorphous polymer

in the physical state of the PET resin as a result of drying and annealing treatments and to relate these changes to the resultant fracture toughness and fatigue crack propagation response. Investigations of this type have been attempted previously on PET[20–22], but these studies never completely isolated and identified the respective roles of crystalline perfection, spherulite size, hydrolysis and tie-molecule density on mechanical behaviour.

This investigation uses the Hoffman regimes as a guideline for establishing lamellar morphologies. For PET, the transition between regime I/II and regime III morphologies occurs at approximately 165°C[23]. Thus, crystallizing PET at 120°C should produce a variable-cluster, crystalline conformation with a high tie-molecule density. In contrast, further annealing some of these samples at 200°C should perfect the lamellae and reduce the tie-molecule density.

In addition, PET, when stored at normal humidity levels, contains 0.3–0.7 wt% water[24] which could potentially lead to hydrolysis during elevated-temperature annealing. In contrast, the concentration of water which is required to equilibrate PET to a molecular weight of 20 500 is calculated to be 0.002%[25,26]. Therefore, annealing is performed under vacuum in order to remove this excess water. *Table 1* provides the diffusivities of water and corresponding times to dry a plaque of PET 3.2 mm thick from a water concentration of 0.4% down to 0.002%[27], as well as rates of hydrolysis[13] at several different temperatures. At 200°C, the rate of hydrolysis

Table 1 Drying and hydrolysis data for PET[25–27]

Temperature (°C)	Diffusivity of H_2O in PET ($cm^2\ s^{-1}$)	Drying time (h)	Rate of hydrolysis (% links h^{-1})
23	5.345×10^{-9}	2690	4.5×10^{-9}
120	2.63×10^{-7}	55.8	4.4×10^{-3}
200	1.60×10^{-6}	5.6	4.1

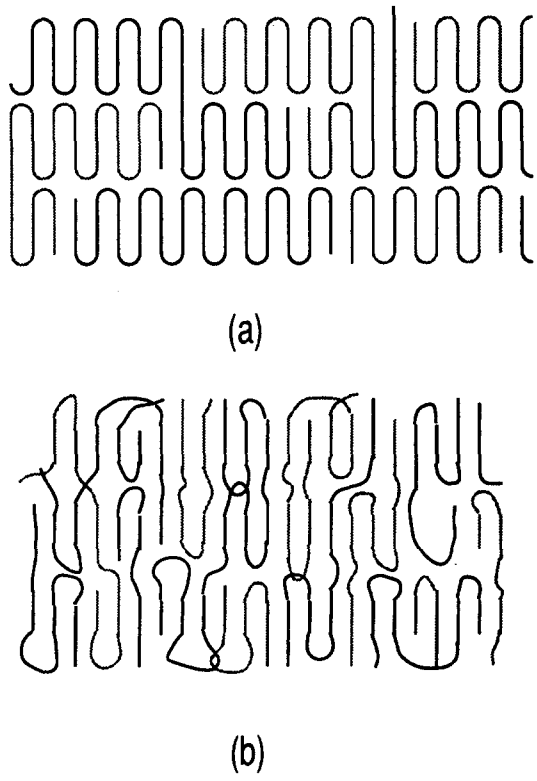

Figure 3 (a) Crystallization at high temperatures is nucleation-limited and produces a regularly folded chain conformation with a low tie-molecule density. (b) Crystallization at low temperatures is diffusion limited and produces a variable cluster chain conformation with a high tie-molecule density

is faster than the rate of drying; at 120°C, however, drying would be completed with little attendant hydrolysis. It is possible, therefore, to examine the high-temperature lamellar structure of PET by vacuum drying samples at 120°C for 120 h before increasing the vacuum annealing temperature to 200°C. Furthermore, additional samples can be annealed in air at 200°C, and compared with the vacuum-annealed samples in order to determine the influence of hydrolysis on the fracture toughness of annealed PET.

Finally, all samples in this study are annealed from an initial amorphous state. Isothermal crystallization from the melt would affect not only the lamellar conformation, but also the macroscopic spherulitic structure[4,9,15,28,29] (see *Figure 2*). Polymers containing large spherulites are susceptible to interspherulitic failure, thereby degrading the resultant mechanical properties and masking the beneficial effects of the interlamellar tie molecules[1,4,30,31]. Quenching to the amorphous state refines the spherulitic nucleation density; as a consequence, the use of amorphous plaques as starting material eliminates the influence of spherulite size on mechanical properties.

EXPERIMENTAL

Material and heat treatments

The PET used in this study was Goodyear 7202 resin, supplied in amorphous, injection-moulded plaques with dimensions 155 × 155 × 3.2 mm. The samples were initially saturated with ~0.4% water; water contents were determined by measuring differences in plaque weight before and after vacuum drying.

Vacuum annealing and drying were performed in standard vacuum box-ovens. Certain samples were vacuum annealed at 120°C and designated as 120V. (Note that heat-treatment times are provided, when required, following the temperature designation. Thus a sample annealed at 120°C for 9 h is designated 120V,9h.) Other samples were vacuum dried at 120°C for 120 h prior to a vacuum anneal at 200°C (200V-D). Samples experiencing this two-step thermal treatment were kept in the vacuum oven throughout both procedures. Air-annealed samples (200A) were inserted into standard atmospheric box-ovens in the as-received, water-saturated condition and annealed at 200°C. Finally, one sample was vacuum annealed at 200°C, but without prior drying (200V-ND).

Physical measurements

Inherent viscosity (IV) measurements were performed using solutions of 1 g polymer in 100 ml of a 75% methylene chloride/25% trifluoroacetic acid mixture. Molecular weights were calculated from equation (1)[32]:

$$M_n = 30\,609(IV)^{0.74} \quad (1)$$

Differential scanning calorimetry (d.s.c.) was performed on a Mettler TA3000 balance, calibrated with indium. Analyses were performed on 5–15 mg samples, sliced from the bulk material. Tests were run from 50 to 290°C, and in flowing nitrogen. The integration baseline for the evaluation of heats of fusion was selected as a straight line from 100 to 280°C[33–35]. The true metastable melting peak (T'_m) for the annealed crystalline structure was taken as the lower-temperature endotherm. The high-temperature endotherm present in all the scans, and the exotherm observed in the scan of the amorphous material are artefact peaks produced by continuous melting and recrystallization of the polymer during the scan[28,36,37]. The value for the theoretical 100% crystalline heat of fusion, used to determine percentage crystallinity, was 136 J g^{-1}, based on calculations by Starkweather *et al.*[38]; this value is similar to those measured in other studies[33,34].

Fracture toughness testing

Fracture toughness tests were performed on notched three-point bend samples, loaded in displacement control at a rate of 10 mm min^{-1} in an Instron servohydraulic test frame. At least five specimens of each annealing condition were tested. Specimens were machined from the annealed plaques to a span of 51 mm, a width of 12.7 mm and a thickness of 3.2 mm. Machined notches were sharpened by sawing with a razor-blade to a total depth of 6.4 mm. Fracture toughness (K_c) values were calculated from the maximum load of the associated load–displacement plot in correlation with the compliance-calculated, instantaneous effective-crack length, in accordance with ASTM E561[39]. Y-calibration and compliance functions were obtained from ASTM D5045[40].

Fatigue testing

Fatigue crack propagation studies were conducted on standard compact tension samples, as per ASTM E647[41], using an Instron servohydraulic closed-loop testing machine. At least two specimens of each annealing condition were tested. Fatigue tests were controlled by by an IBM computer in conjunction with software written by Fracture Toughness Associates[42]. Crack lengths were measured by compliance techniques (within the computer program) and confirmed by visual observation with a Gaertner travelling microscope. All waveforms were sinusoidal with an R-ratio (K_{min}/K_{max}) of 0.1, except where noted. Relations of compliance and Y-calibration to crack length were provided in the controlling computer software[42].

Crack growth rates were correlated with ΔK using the Paris relation[2]

$$da/dN = A\Delta K^m \quad (2)$$

where A and m are material constants that depend also on test variables such as frequency and environment. All tests were conducted at a frequency of 5 Hz, in laboratory air at ambient temperature. Crack tip temperatures were monitored with a Barnes model RM-2B infra-red travelling microscope; no significant rise in temperature at the crack tip was noted.

Fractography

Electron fractography was performed on an ETEC scanning electron microscope at an accelerating voltage of 5 kV. The samples were coated with gold–palladium prior to examination. Fracture profiles were photographed using transmitted light on a Zeiss metallograph at 100 × magnification.

RESULTS AND DISCUSSION

Physical properties

Inherent viscosity (IV) values for the PET samples are plotted in *Figure 4* as a function of annealing time, and

are listed in *Table 2* along with associated molecular weights. Note that the coefficients of variation for these values do not exceed 2%. For the initial-state, amorphous material, IV is measured to be 0.58. This IV value remains constant for the samples vacuum-annealed at 120°C for up to 120 h (120V samples); at 120°C, drying occurs faster than hydrolysis and there is no change in the degree of polymerization.

IV values for the samples annealed at 200°C are, however, strongly affected by the corresponding water concentration. The air-annealed (200A) samples experience a significant drop in IV; this drop can be related to hydrolysis of the polymer with the retained water. Similarly, the sample vacuum annealed at 200°C without prior drying (200V-ND) also experiences a drop in IV. As predicted, the water in the 200V-ND sample did not diffuse out quickly enough to prevent hydrolysis. By contrast, IV values for the 200V-D,9h and 200V-D,24h samples (annealed at 200°C after drying at 120°C for 120 h) remain the same as the value for the material annealed at 120°C. Thus, the prior drying of these samples did remove enough water to prevent hydrolysis. (When examining plots of the data, note that the 200V-D,0h datum is the same as the 120V,120h datum.) In addition, vacuum-annealing of the 200V-D samples for longer times removed enough additional water for the IV to increase through solid-state polymerization. Nonetheless, since the IV does not increase significantly until at least 24 h of annealing at 200°C, the 200V-D,9h sample can be used to examine the influence of high-temperature crystalline conformation of non-hydrolysed material on mechanical response.

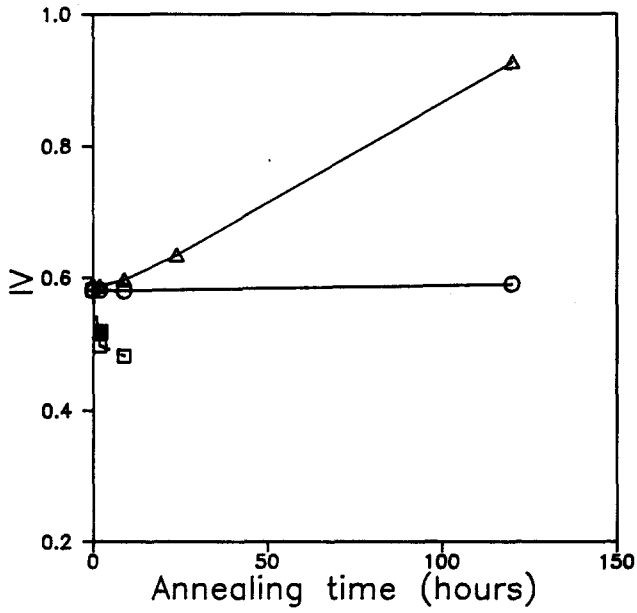

Figure 4 Inherent viscosity (IV) plotted *versus* annealing time for annealed PET. (○) 120V, (△) 200V-D, (□) 200A, (■) 200V-ND

D.s.c. scans for the vacuum-annealed samples are shown in *Figure 5*, whereas d.s.c. scans for air-annealed samples were found to be identical with their vacuum-annealed counterparts. A composite plot of all the metastable melting temperature (T'_m) values is provided in *Figure 6*, and heats of fusion (ΔH) for the vacuum-annealed material are plotted in *Figure 7*. Coefficients of variation for the T'_m and ΔH values do not exceed 1 and 5%, respectively. (T'_m, ΔH and percentage crystallinity values are also shown in *Table 2*.) Note that T'_m, related to the annealed structure, is associated with the lower-temperature endotherm in each of the scans in *Figure 5*. The peak at 260°C, which appears in all the scans, including that for the amorphous material, is an artefact of the scan, produced by repeated melting and crystallization of the polymer during the scan itself[28,36,37]; this peak represents the melting temperature of completely perfected PET.

Figures 5–7 show that increasing the annealing time and temperature increases both the metastable melting temperature (T'_m) and the heats of fusion. In order for an annealing process to reduce the total free energy of a polymer system, the number of crystal imperfections and the volume fraction of amorphous material must decrease[9]. Tie molecules, which represent one type of

Table 2 Physical property data for amorphous and annealed PET

Sample conditions	Inherent viscosity (IV)	Number-average molecular weight (M_n)	Metastable melting peak (T'_m) (K)	Heat of fusion (ΔH) ($J\,g^{-1}$)	Crystallization (%)
Amorphous	0.581	20 500	–	0	0
120V					
20 min	0.584	20 500	–	28	21
2 h	0.582	20 500	137	49	36
9 h	0.582	20 500	144	49	36
120 h	0.591	20 700	146	50	37
200V-D					
0 h	0.591	20 700	146	50	37
2 h	0.587	20 600	219	62	45
9 h	0.597	20 900	230	65	48
24 h	0.631	21 800	233	70	51
120 h	0.927	28 900	262	83	61
200A					
2 h	0.497	18 200	219	62	45
9 h	0.482	17 800	230	65	48
200V-ND					
2 h	0.519	18 800	219	62	45

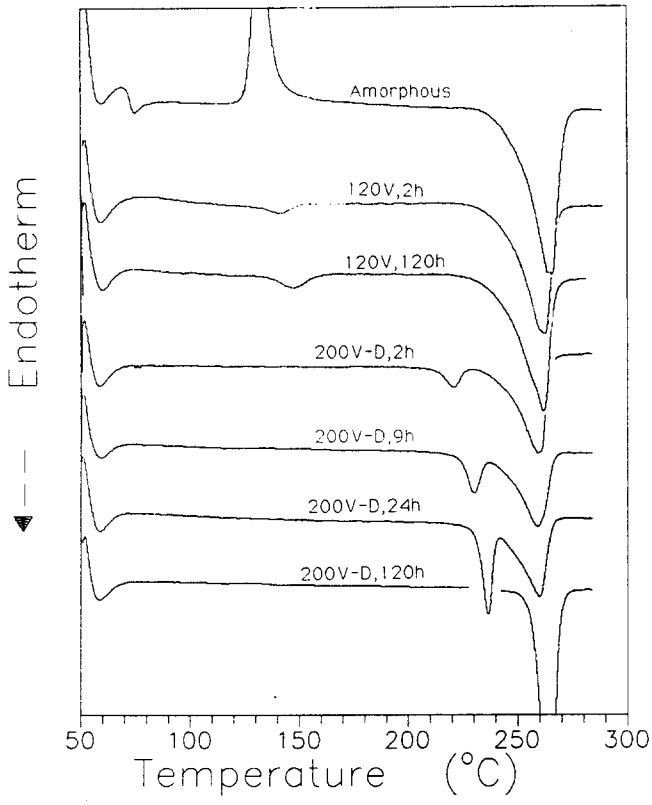

Figure 5 D.s.c. traces for vacuum-annealed PET. True T'_m values are measured at the low-temperature endotherms. All other endotherms and exotherms are produced by continuous crystallization and melting of the polymer during the scan

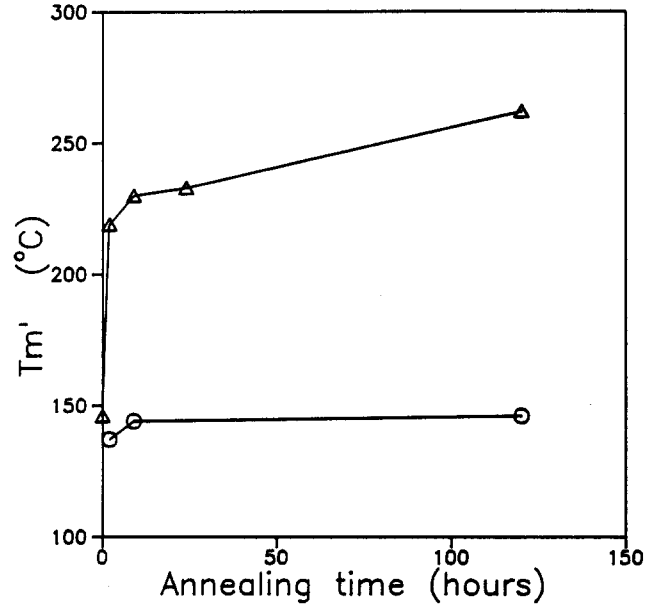

Figure 6 Metastable phase melting temperatures of the annealed PET, plotted as T'_m *versus* annealing time. These plots are representative of both vacuum- and air-annealed material. (○) Annealed at 120°C, (△) annealed at 200°C

imperfection, are 'reeled in' to allow development of the more perfect, regularly folded lamellar conformation (*Figure 3*)[11,17]. As these imperfections are removed, the perfected crystals melt at increasingly higher temperatures, whereby the increased T'_m values as noted in *Figure 6*[28,29,43] reflect a reduction in tie-molecule density associated with annealing. This reeling in of chain segments results in fewer tie molecules meandering between the lamellae and should reduce material toughness.

In addition, as the lamellae become perfected, they thicken and encroach upon the interlamellar amorphous regions. As the amorphous volume decreases, the corresponding volume fraction of crystallinity increases. The increase in the total heat of fusion, associated with increasing annealing time and temperature, simultaneously reflects increased crystallinity, increased lamellar perfection and decreased tie-molecule density (*Figure 7*)[28,29,43].

Other experimental techniques have been used to analyse the conformational changes which occur when PET is annealed. Annealing intensifies the infra-red peak produced by the crystalline *trans* isomer in PET[44,45]. The crystalline *trans* isomer is associated with a regularly folded conformation. Simultaneously, the infra-red peak produced by the amorphous *trans* isomer decreases; this phenomenon can be associated with a decrease in the number of tie molecules. An increase in chain mobility, directly related to the increasing annealing temperature, is believed to cause this transformation from the amorphous to crystalline *trans* isomer. Indeed, the number of crystalline *trans* isomers is observed to increase significantly when annealing occurred above 160°C, which is close to the temperature of the regime II–III transition[23].

Annealing of PET will also cause a decrease in the width of the scattering intensity obtained from small-angle X-ray scattering experiments. This decrease in width of scattering peak is associated with a thickening of the crystal lamellae due to increased perfection[1,28,29]. In addition, small-angle neutron scattering studies have also detected conformational rearrangement to more ordered structures in PET annealed in regime I/II[46,47]. As noted previously, increasing conformational perfection should reduce the tie molecule density and result in lower toughness.

Fracture toughness

Fracture toughness values for the annealed PET are shown in *Figure 8*; these values vary greatly, depending upon the associated annealing treatment. (The coefficients

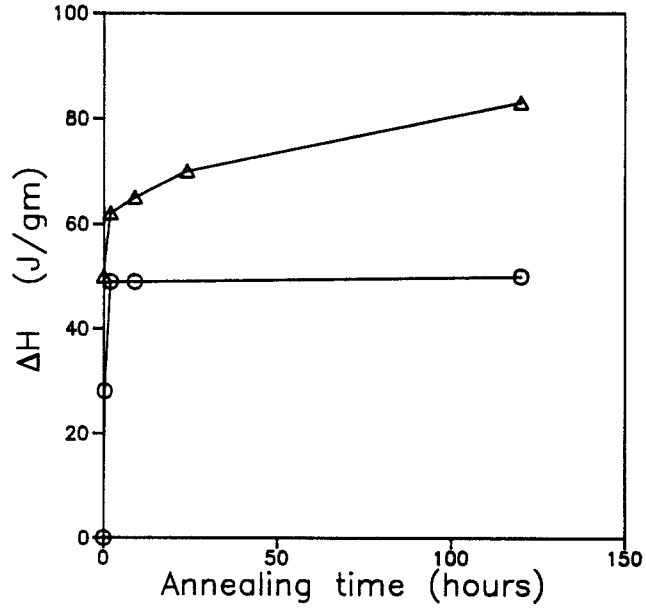

Figure 7 Heats of fusion for annealed PET, plotted as ΔH *versus* annealing time. These plots are representative of both vacuum- and air-annealed material. (○) Annealed at 120°C, (△) annealed at 200°C

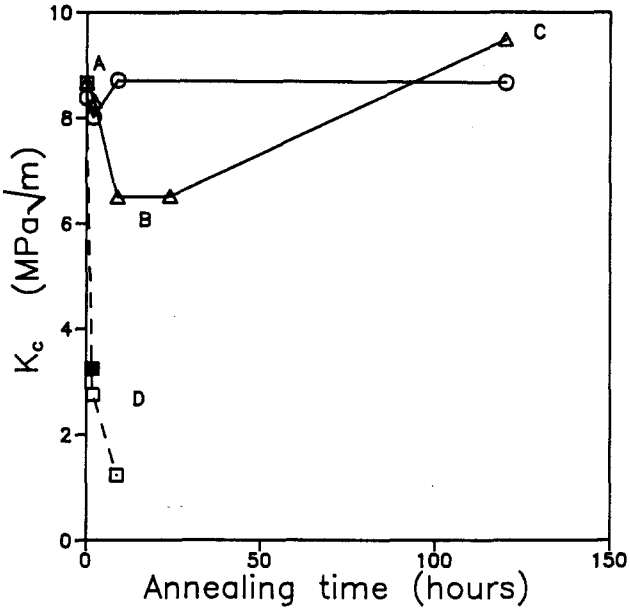

Figure 8 Fracture toughness values of the annealed PET, plotted as K_c *versus* annealing time. Rapid quenching to the amorphous state, crystallizing in regime III, and increasing the molecular weight (path B–C) produce material with high K_c values. Crystallization in regime I/II and hydrolysis produce material with low K_c values (paths A–B and A–D). (○) 120V, (△) 200V-D, (□) 200A, (■) 200V-ND

of variation for the samples annealed at 120 and 200°C are 8 and 16%, respectively.) These trends in toughness values can be explained, however, through correlation with the morphological transformations discussed in the previous section.

Among the highest K_c values for the materials examined in this study are those found for the materials annealed at 120°C. Crystallization of these samples occurs in regime III, whereby the material contains a relatively large concentration of tie molecules (see T'_m and ΔH values in *Figures 6* and *7*); this high tie-molecule density leads to stabilization of the craze structure at the crack tip which produces the high fracture toughness values exhibited in *Figure 8*. The regime III structure does not change significantly in association with annealing between 9 and 120 h and, therefore, toughness values remain constant for the materials annealed for these times.

Fracture toughness levels decrease in the samples experiencing the first 9 h of vacuum annealing at 200°C, reflecting the deleterious effect of decreased tie-molecule density. Annealing at 200°C in vacuum for short times produces no change in molecular weight but leads to a transformation from the regime III crystalline conformation to a more perfect, regime I/II conformation. The tie-molecule density decreases as the amount of regular folding increases, as evidenced by increasing T'_m and heat of fusion values (*Figures 6* and *7*), whereby toughness is reduced through a reduction in the crack tip craze network.

Fracture toughness values increase, however, as the vacuum annealing time at 200°C is increased to 120 h; during this time period, the associated reduction in water content is accompanied by extension of the polymerization process (recall the increase in *IV* during this time period; see *Figure 4*). Since the solid-state polymerization process occurs mainly in the interlamellar region of a semicrystalline material, tie-molecule density is increased. The high tie-molecule density stabilizes the craze network at the crack tip, whereby the K_c value for the 200V-D, 120h sample is high, even though the sample is annealed at a regime I/II temperature.

The lowest fracture toughness values observed during this study are associated with samples annealed at 200°C without prior drying (200V-ND and 200A). These test samples were initially saturated with water such that annealing at 200°C brought about a significant hydrolysis reaction (noted by a reduction in IV; *Figure 4*) that is focused in the interlamellar amorphous region. In addition, annealing PET at 200°C produces a more perfect conformation; the combination of these two effects (hydrolysis and perfected conformation) greatly reduces tie-molecule density, thereby resulting in a dramatic reduction in toughness.

Finally, it should be noted that the K_c value for the amorphous PET is also high (8.4 MPa $m^{1/2}$). In the amorphous state, molecular slip is less restrained since the chains are not tightly bound into lamellae. Therefore, in amorphous PET at room temperature, gross shear yielding is the preferred deformation mechanism[1,48,49] that leads to a low yield strength, high ductility and the resultant ability to form extensive plastic deformation at the crack tip. The high K_c value for the amorphous PET is a direct result of this large shear damage zone, which represents a large amount of blunting.

Fracture surface appearance

Fractographs and damage profiles, shown in *Figures 9* and *10*, respectively, confirm the different deformation mechanisms which control the toughness in PET. *Figure 9a* shows evidence for shear deformation (shear lips) in the amorphous PET; in the 120V,120h sample (*Figure 9b*), however, the extent of shear lip development is reduced and a craze morphology is observed. In *Figure 10a* and *10b*, the high-toughness 120V,120h and 200V-D,120h samples display extensive damage at the crack tip, related to multiple crazing due to a high tie-molecule density. In the low toughness materials (200V-D,9h and 200A materials; *Figures 10c* and *d*, respectively), the craze network is much smaller due to the decrease in tie-molecule density. The factors which affect the fracture toughness of PET are summarized in *Table 3*.

Fatigue crack propagation behaviour

As with toughness response, resistance to fatigue crack propagation (FCP) is also affected by annealing conditions, as shown in *Figure 11*. PET annealed at 120°C is the most fatigue-resistant material tested in this study, reflecting its regime III crystallization morphology. Solid-state polymerization in the 200V-D,120h sample also produces a highly fatigue-resistant material. In contrast, the 200V-D,9h sample exhibits reduced FCP resistance due to the resin's regime I/II crystallization morphology.

Variations in fatigue resistance reflect the different craze structures associated with each annealing condition. In the 200V-D,9h sample, the crack is observed to follow a single craze (see *Figure 12*). Single craze growth – a result of low tie-molecule density produced by the regularly folded conformation – produces a small damage zone with little blunting, which leads to the inferior FCP resistance of this material[50,51]. Alternatively, a high

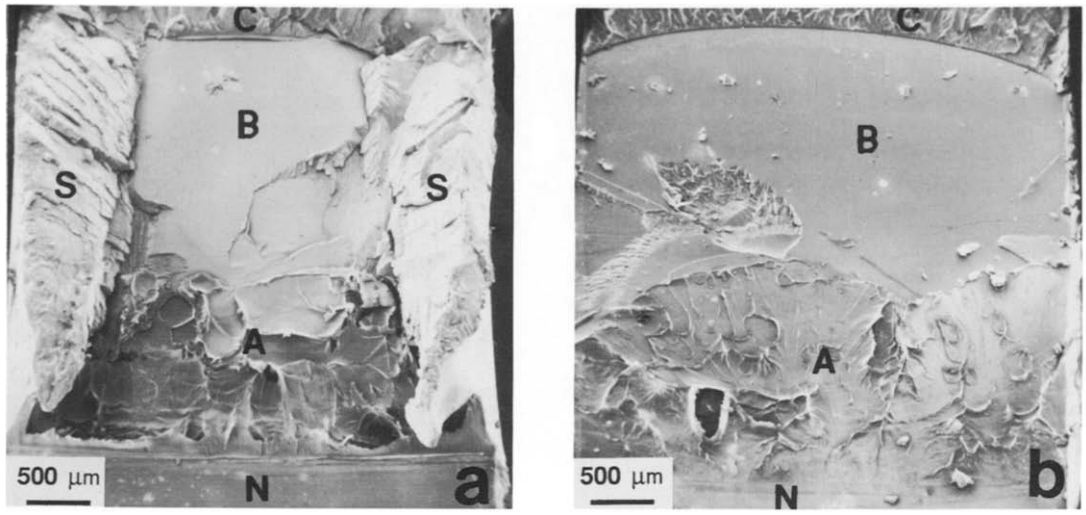

Figure 9 Fracture surfaces of (a) amorphous and (b) semicrystalline PET, showing regions of slow crack growth (region A), rapid fracture through the developing craze (region B) and brittle fracture beyond the craze tip (region C). (a) Shear lip formation (S) is extensive in the amorphous material. (b) No shear lips are found in the semicrystalline material (120V,120h). (The notch region is N. The nominal crack growth direction is from bottom to top in each figure)

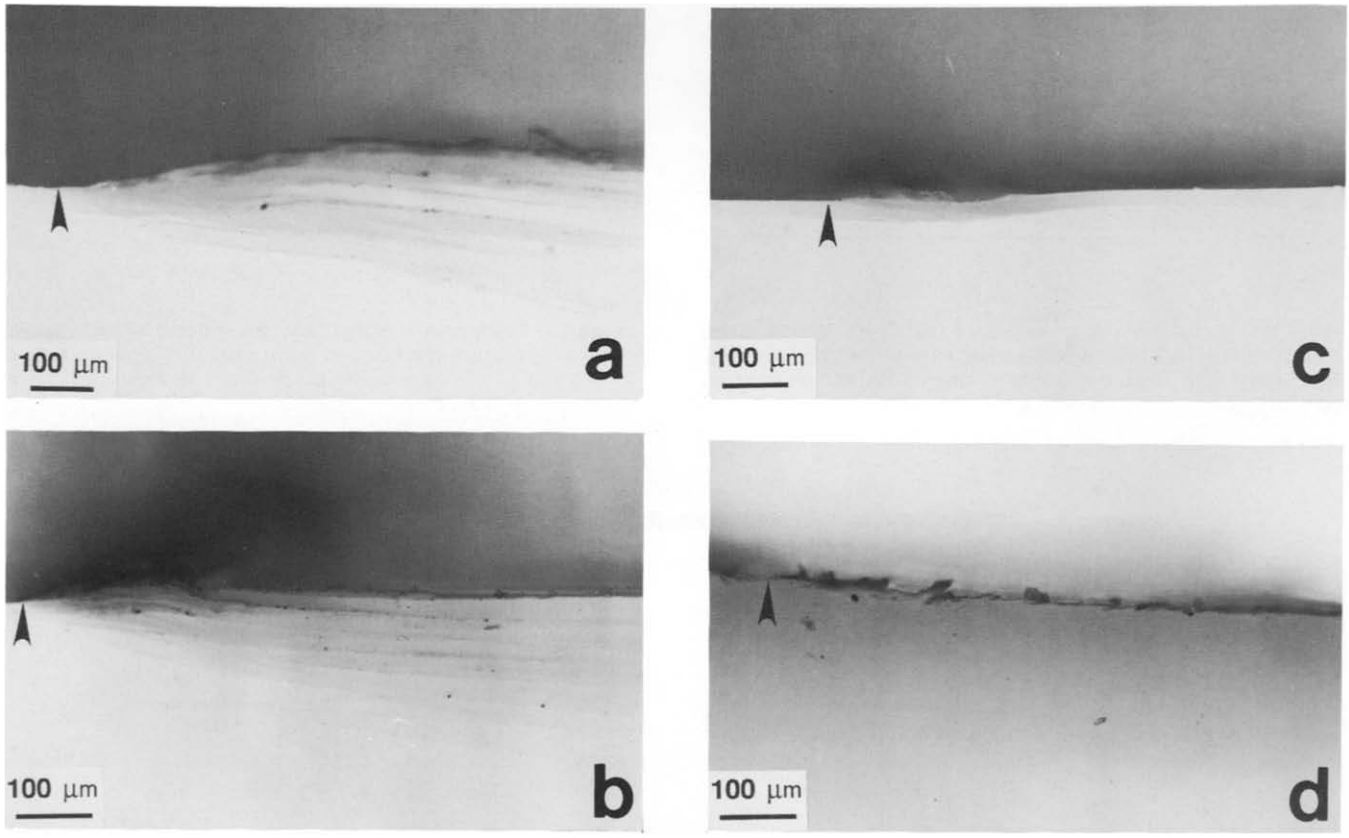

Figure 10 Fracture profiles for the semicrystalline PET. Extensive damage is sustained in the (a) 120V,120h and (b) 200V-D,120h materials leading to high toughness. Little damage is observed in the (c) 200V-D,9h and (d) 200A samples associated with low toughness material. (Arrows indicate the initial notch location. The nominal crack growth direction is from left to right in each figure)

tie-molecule density, resulting from either regime III crystallization or solid-state polymerization, produces a stable, fatigue-resistant craze network in both the 120V,120h and 200V,120h samples, respectively (see *Figure 13*). A multiple-craze network at the crack tip is effectively more blunt than a single craze; as a result, the stress is less intense at the crack tip, whereby the rate of crack growth becomes slower for a given applied driving force (ΔK).

Scatter in the FCP curves is also related to the craze structure found in each material. The 200V-D,9h sample displays continuous growth rate response with little associated scatter. Such behaviour results from normal crack growth in the wake of a single craze (see *Figure 12*). In contrast, the FCP curve for the 120V,120h sample is jagged, resulting from the growth mechanism shown in *Figure 13*. (Note that this jagged behaviour has also been observed in poly(butylene terephthalate)

(PBT)[52].) The crack in this model is initially sharp, and is surrounded by a large multiple-craze damage zone (*Figure 13a*). As the sample is cycled, the damage zone increases while the physical crack blunts (*Figure 13b*); during this period of blunting, the compliance-calculated crack growth rate decelerates. After additional cycles, several of the crazes within the multiple-craze zone thicken and eventually open (this opening allows flashes of light to transmit through the sample at each of the crazes). The crack tip is now diffuse and composed of multiple craze/cracks (*Figure 13c*). Eventually, one of these opened crazes/cracks develops into the main crack, thereby resulting in acceleration of the compliance-calculated growth rate (*Figure 13d*). The newly sharpened crack then blunts again, thereby slowing the growth rate; at this point, the entire fatigue fracture process is repeated.

In the present study, significant stable fatigue crack growth is possible in samples annealed at 200°C for up to 120 h. However, in a prior investigation of FCP in annealed PET[22,53], material annealed at 200°C for only

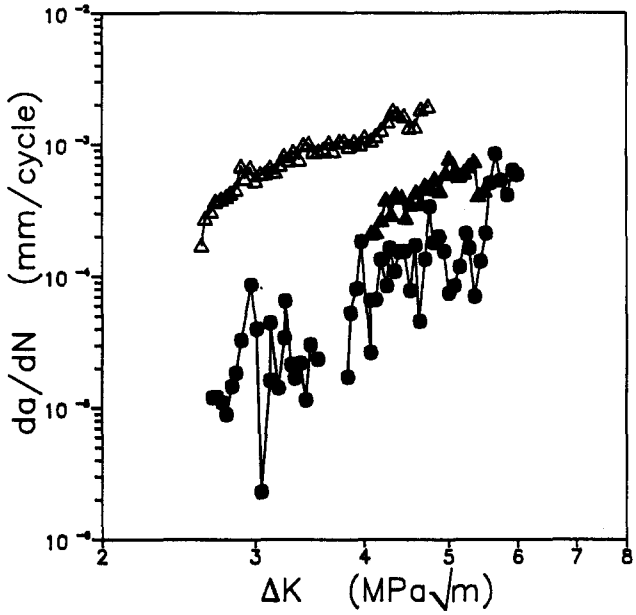

Figure 11 Fatigue crack propagation data for the annealed semicrystalline PET. Fatigue resistance is improved by increasing the tie-molecule density (120V,120h and 200V-D,120h samples). (●) 120V,120h, (△) 200V-D,9h, (▲) 200V-D,120h

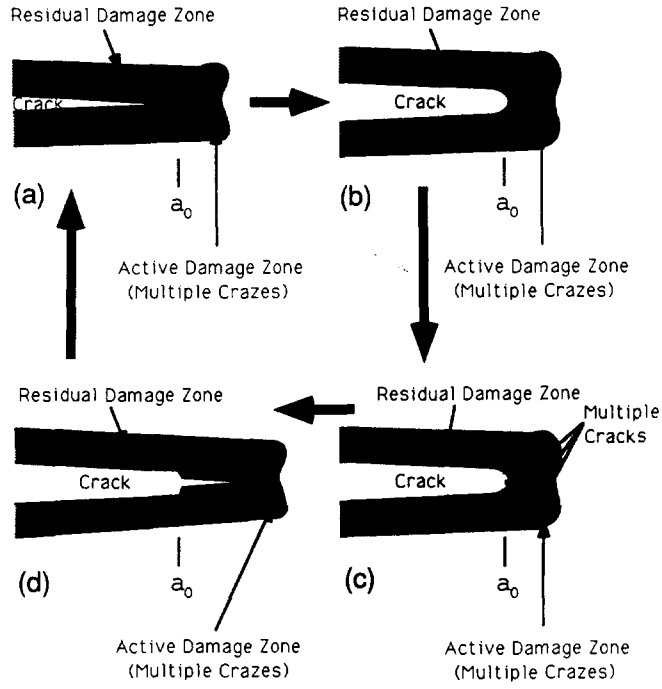

Figure 13 Crack growth in the 120V,120h material follows a pattern of blunting, multiple-cracking and resharpening. This pattern requires many loading cycles to complete and produces the jagged appearance of the associated FCP plot

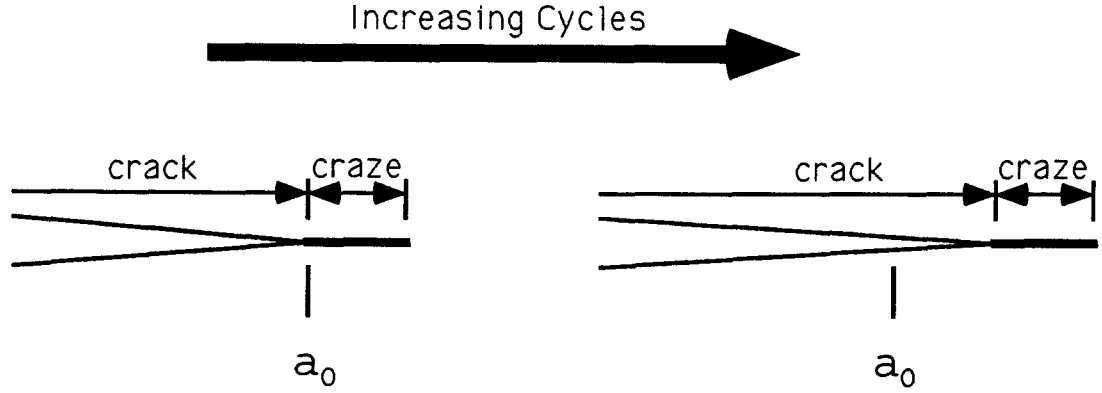

Figure 12 Scheme showing normal crack growth following in the wake of a single craze. This behaviour is observed in the 200V-D,9h material

Table 3 Summary of fracture mechanisms for amorphous and annealed PET

Condition	Crystallization (%)	M_n	Blunting mechanism	K_c (MPa m$^{1/2}$)	Primary factor affecting K_c
Amorphous	0	20 500	Large shear yield zone	8.4	Material is amorphous
120V,120h	37	20 700	Extensive multiple crazing	8.7	Material is crystallized in regime III
200V-D,9h	48	20 900	Limited crazing	6.5	Material is crystallized in regime I/II
200V-D,120h	61	28 900	Extensive multiple crazing	9.5	Solid state polymerization occurs
200A,9h	48	17 800	Very limited crazing	1.2	Hydrolysis occurs

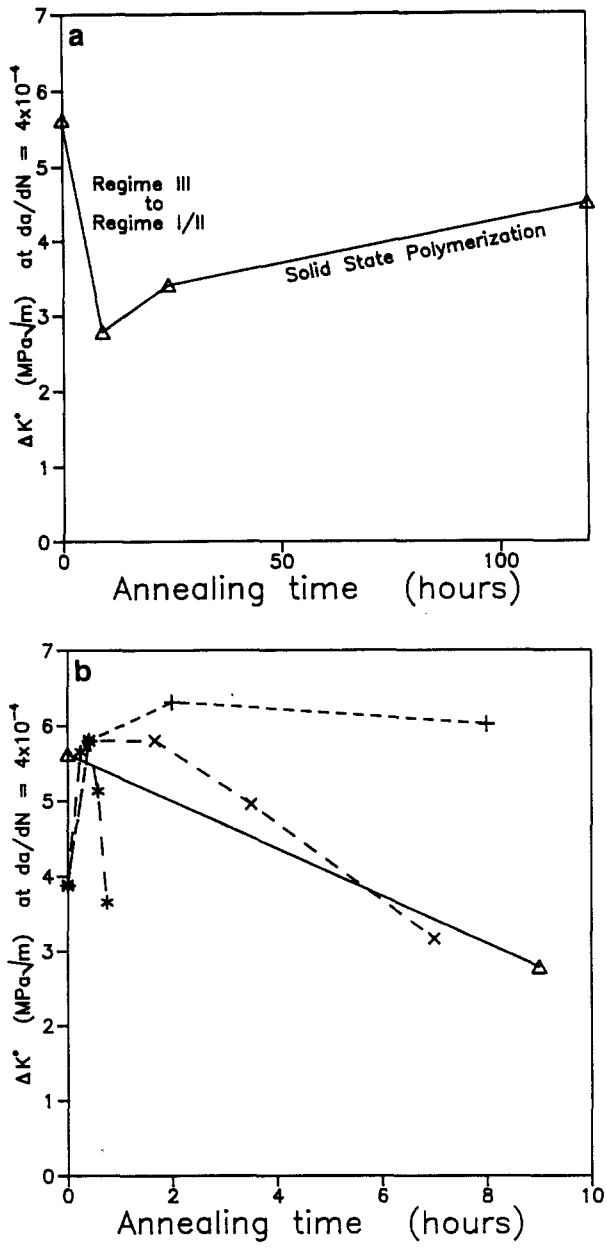

Figure 14 (a) Relation between crack driving force and annealing time for dry PET annealed at 200°C in vacuum. ΔK^* corresponds to the crack driving force required to produce a growth rate of 4×10^{-4} mm/cycle. The initial decrease in ΔK^* is due to transformation from regime III (high tie-molecule density) conformation to regime I/II (low tie-molecule density) conformation. The subsequent increase in ΔK^* is associated with an increased tie-molecule density resulting from solid-state polymerization. (b) ΔK^* *versus* annealing time for the annealed PET in the Ramirez investigation[22,53] ($M_n = 28\,000$). (+) Annealed at 120°C, (×) annealed at 152°C, (*) annealed at 200°C. Note that FCP resistance degrades rapidly with increasing annealing temperature and that the material vacuum-annealed at 200°C in this investigation (△) is also plotted for comparison

2 h became too brittle to sustain stable FCP. *Figure 14a* traces the change in fatigue resistance of the samples annealed at 200°C by plotting ΔK^* (driving force required to produce a growth rate of 4×10^{-4} mm/cycle) *versus* annealing time. A plot of ΔK^* *versus* annealing time for the samples in the Ramirez study[22,53] (see *Figure 14b*), reveals that the crack driving force drops severely with increasing annealing times and temperatures above 120°C.

It is interesting to note that the number-average molecular weight of the material in the Ramirez study is 28 000[22], which is greater than the molecular weight of the material in the present study (20 500). Nonetheless, the fatigue behaviour for the former material is worse than that for the material in the present study. This seemingly contradictory result can be rationalized by the presumption that hydrolysis must have occurred in the Ramirez samples. If PET is insufficiently dried prior to annealing at elevated temperatures (as with the 200A,9h sample of the present investigation), the associated hydrolysis reaction that occurs rapidly within the amorphous interlamellar regions during annealing would severely reduce the number of available tie molecules. With such a low tie-molecule density, samples dried in air and annealed at 200°C would be too brittle to sustain stable fatigue crack growth. The material in Ramirez's investigation was 'dried' by merely storing the material in a desiccator for 15 h[22]. This technique, theoretically, could not have removed a sufficient amount of water from the virgin resin, and led to the reported evidence of hydrolysis[22]. The results of this investigation would, therefore, suggest that the inferior FCP behaviour noted by Ramirez with his supply of annealed material was due to hydrolytic reduction of the tie-molecule density.

CONCLUSIONS

Altering the molecular conformation of PET by annealing at different Hoffman crystallization temperatures significantly affects the polymer's physical properties and fracture behaviour.

1. The structure of the amorphous state favours widespread shear yielding, and produces a tough, ductile polymer.
2. Crystallizing the polymer restricts shear yielding, whereby crazing becomes the preferred deformation mechanism.
3. Annealing at a Hoffman regime III crystallization temperature, or increasing the molecular weight through solid-state polymerization, produces material with a high tie-molecule density; consequently, high toughness results from the formation of a stable craze network.
4. Annealing in regime I/II perfects the lamellae and reduces the tie-molecule density. The craze network becomes less stable and the toughness decreases.
5. Air-annealing at 200°C will both hydrolyse the material and perfect the crystals. The combination of these two effects greatly reduces the tie-molecule density and produces the lowest toughness material of those examined in this study.
6. FCP resistance is improved by crystallization at low temperatures (in regime III) or by increasing the molecular weight in association with annealing at 200°C in vacuum. Conversely, fatigue resistance is degraded by hydrolysis and/or crystallizing at higher temperatures (in regime I/II).

ACKNOWLEDGEMENTS

The authors wish to thank Dr Mike Carling at DuPont for his assistance during this investigation. In addition, many hours of technical discussions with Dr Tom Clark were very helpful. This work was funded by the E.I. DuPont deNemours Corporation.

REFERENCES

1 Kinloch, A. J. and Young, R. J. 'Fracture Behavior of Polymers', Applied Science Publishers, Barking, 1983
2 Hertzberg, R. W. 'Deformation and Fracture Mechanics of Engineering Materials', 3rd Edn, Wiley, New York, 1989
3 Kausch, H. H. 'Polymer Fracture', Springer, Berlin, 1978
4 Schultz, J. M. *Polym. Eng. Sci.* 1984, **24**, 770
5 Friedrich, K. *Adv. Polym. Sci.* 1983, **52/53**, 225
6 McReady, M. J., Schultz, J. M., Lin, J. S. and Hendricks, R. W. *J. Polym. Sci., Polym. Phys. Edn* 1979, **17**, 725
7 deCharentenay, F. X., Laghouati, F. and Dewas, J. In 'Proc. Conference on Deformation, Yield and Fracture', Plastics Rubber Institute, London, 1979, Vol. 4, p. 6.1
8 Yeh, Y. T. and Runt, J. *J. Mater. Sci.* 1989, **24**, 2637
9 Wunderlich, B. 'Macromolecular Physics', Academic Press, New York, Vol. 1, 1973 and Vol. 2, 1976
10 Odian, G. 'Principles of Polymerization', Wiley, New York, 1981
11 Miyagi, A. and Wunderlich, B. *J. Polym. Sci., Polym. Phys. Edn* 1972, **10**, 2085
12 Miyagi, A. and Wunderlich, B. *J. Polym. Sci., Polym. Phys. Edn* 1972, **10**, 2073
13 McMahon, W., Birdsall, H. A., Johnson, G. R. and Camilli, C. T. *J. Chem. Eng. Data* 1959, **4**, 57
14 Jabarin, S. A. and Lofgren, E. A. *Polym. Eng. Sci.* 1984, **24**, 1056
15 Sperling, L. H. 'Introduction to Physical Polymer Science', Wiley, New York, 1986
16 Hoffman, J. D., Davis, G. T. and Lauritzen, J. I. in 'Treatise on Solid State Chemistry', Vol. 3, Plenum Press, New Yok, 1976, Ch. 7
17 Hoffman, J. D. *Polymer* 1982, **23**, 656
18 Hoffman, J. D. *Polymer* 1983, **24**, 3
19 Clark, E. J. and Hoffman, J. D. *Macromolecules* 1984, **17**, 878
20 Dixon, E. R. and Jackson, J. B. *J. Mater. Sci.* 1968, **3**, 464
21 Foot, J. S. and Ward, I. M. *J. Mater. Sci.* 1972, **7**, 367
22 Ramirez, A. *PhD Dissertation*, Lehigh University, Bethlehem, USA, 1982
23 Phillips, P. J. and Tseng, H. T. *Macromolecules* 1989, **22**, 1649
24 Jabarin, S. A. and Lofgren, E. A. *Polym. Eng. Sci.* 1986, **26**, 620
25 Pecorini, T. J. *PhD Dissertation*, Lehigh University, Bethlehem, USA, 1992
26 Sawada, H. 'Thermodynamics of Polymerization', Marcel Dekker, New York, 1976
27 Hubbell, W. H., Brandt, H. and Munir, Z. A. *J. Polym. Sci.* 1975, **13**, 493
28 Groeninckx, G., Reynaers, H., Berghmans, H. and Smets, G. *J. Polym. Sci., Polym. Phys. Edn* 1980, **18**, 1311
29 Groeninckx, G. and Reynears, H. *J. Polym. Sci., Polym. Phys. Edn* 1980, **18**, 1325
30 Way, J. L., Atkinson, J. R. and Nutting, J. *J. Mater. Sci.* 1974, **9**, 299
31 Greco, R. and Ragosta, G. *J. Mater. Sci.* 1988, **23**, 4171
32 Carling, M. J. Personal communication, August 1989
33 Blundell, D. J., Beckett, D. R. and Willcocks, P. H. *Polymer* 1981, **22**, 704
34 Illers, K. H. *Colloid. Polym. Sci.* 1980, **258**, 117
35 Lin, S.-B. and Koenig, J. L. *J. Polym. Sci. Polym. Symp.* 1984, **71**, 121
36 Blundell, D. J. *Polymer* 1987, **28**, 2248
37 Sweet, G. E. and Bell, J. P. *J. Polym. Sci. A-2* 1972, **10**, 1273
38 Starkweather, H. W., Zoller, P. and Jones, G. A. *J. Polym. Sci., Polym. Phys. Edn* 1983, **21**, 295
39 ASTM E561-86, Standard Practice for R-Curve Determination, 'Annual Book of ASTM Standards', ASTM, Philadelphia, 1988
40 ASTM D5045-91, Standard Test Method for Plane-Strain Fracture Toughness and Strain Energy Release Rate of Plastic Materials, 'Annual Book of ASTM Standards', ASTM, Philadelphia, 1991
41 ASTM E647-88, Standard Test Method for Measurement of Fatigue Crack Growth Rates, 'Annual Book of ASTM Standards', ASTM, Philadelphia, 1988
42 'FCGR2 Users Reference Manual', Fracture Technology Associates, Pleasant Valley, 1986
43 Roberts, R. C. *Polymer* 1969, **10**, 117
44 Lin, S.-B. and Koenig, J. L. *J. Polym. Sci., Polym. Phys. Edn* 1983, **21**, 2365
45 Lin, S.-B. and Koenig, J. L. *J. Polym. Sci., Polym. Phys. Edn* 1982, **20**, 2277
46 Gilmer, J. W., Wiswe, D., Zachmann, H.-G., Kugler, J. and Fisher, E. W. *Polymer* 1986, **27**, 1391
47 McAlea, K. P., Schultz, J. M. and Gardner, K. H. *J. Polym. Sci., Polym. Phys. Edn* 1987, **25**, 651
48 Kastelic, J. R. and Baer, E. *J. Macromol. Sci. – Phys.* 1973, **B7**, 679
49 Stearne, J. M. and Ward, I. M. *J. Mater. Sci.* 1969, **4**, 1088
50 Takemori, M. T., Morelli, T. A. and McGuire, J. *J. Mater. Sci.* 1989, **24**, 2221
51 Williams, J. G. 'Fracture Mechanics of Polymers', Ellis Horwood, Chichester, 1987
52 Cheng, W. M. and Carling, M. J. unpublished work, Lehigh University, Bethlehem, USA, 1985
53 Ramirez, A., Gaultier, P. M., Mason, J. A. and Hertzberg, R. W. in 'Fatigue in Polymers', Plastics and Rubber Institute, London, 1983, p. 31